A Multi Parameter Synchronous Identification Method for Stiffness and Damping of Single Fixed Clamp Based on Pareto Algorithm

Kunpeng Xu

School of Mechanical Engineering and Automation, Northeastern University, Shenyang 110819, China.
Key Laboratory of Vibration and Control of Aerodynamic Equipment, Ministry of Education, Northeastern University, Shenyang 110819, China.

Cheng Xu

Yantai Jereh Oilfield Services Group Co., Ltd., Yantai 264003, China.

Yicheng Liu and Bo Wang

School of Mechanical Engineering and Automation, Northeastern University, Shenyang 110819, China.
Key Laboratory of Vibration and Control of Aerodynamic Equipment, Ministry of Education, Northeastern University, Shenyang 110819, China. E-mail: wangb@me.neu.edu.cn

Yan Shi

AECC Shenyang Liming Aero Engine Corporation Ltd., Shenyang 110043, China.
Northwestern Polytechnical University, Xi'an, 710072, China.

Shaoyang Wang

CPC Liaoning Provincial Party School, Shenyang 110004, China.

(Received 4 June 2024; accepted 3 September 2024)

As a composite structure, the single fixed clamp (SFC) is an important supporting component of the aeroengine piping system. The dynamic parameters (stiffness and damping) of SFC have significant differences in bolt direction and opening direction. Accurately identifying the dynamic parameters of an SFC in both directions is of great significance for the study of pipeline system dynamics. At present, there is very little research on the identification of dynamic parameters for such SFC. Therefore, an SFC-straight pipe structure for identifying the dynamic parameters of an SFC is proposed in this paper. In this structure, one end of the straight pipe is completely fixed, and the other end is supported by an SFC. This structure can better reflect the working state of the SFC. A dynamic model of this structure is established based on the finite element method for parameter identification of SFC. In the finite element model (FEM), the constraint effect of the SFC is simplified into two identical spring-damping groups. Considering the structural asymmetry, spring and damping parameters for bolt direction and opening direction are separately set in each spring damping group. Next, based on the Pareto multi-objective genetic algorithm, an identification algorithm and procedure for the stiffness and damping of the SFC using modal test data as input parameters are proposed. Through experimental testing, parameter identification is carried out for DK8 type SFC, and a straight pipe experimental structure completely supported by two SFCs is constructed to verify the correctness of the identification results.

1. INTRODUCTION

In pipeline systems in fields such as aerospace and aviation, the single fixed clamp (SFC) is widely used as an important pipe support and fixed component.[1–5] In the pipeline system of the aeroengine, a composite structure SFC is commonly used (as shown in Fig. 1), which is composed of steel bands, metal rubber gaskets, and mounting bolts. This SFC not only has the function of fixing and supporting the pipe body but can also reduce the vibration of the pipe body. During the operation of aeroengines, the vibration fatigue damage of the pipeline system can lead to serious flight accidents,[6–9] and the vibration problem of the pipeline system has always been a concern. However, the dynamic parameters (support stiffness and damping) of the SFC have a significant impact on the vibration characteristics of the pipeline system. Therefore, conducting research on the dynamic parameter identification of SFCs is of great significance for the dynamic analysis of pipeline systems. To carry out the identification of dynamic parameters of SFCs in aeroengines to serve the dynamic research of pipeline systems, it is necessary to clarify the dynamic modeling method of pipeline systems and the way in which the dynamic parameters of an SFC are reflected in the model. In recent years, research on dynamic modeling and the analysis of pipeline systems considering SFC support and constraints has received attention.

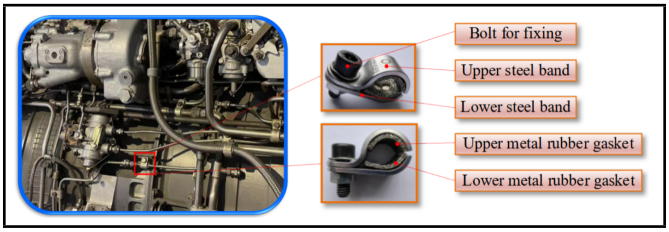

Figure 1. Structure of SFC.

These modeling methods can generally be divided into analytical methods,[10–12] semi-analytical methods,[13–15] finite element methods,[16–22] transfer matrix methods,[23–27] etc.

To make the identification of dynamic parameters of SFC better serve the dynamic research of pipeline systems, it is necessary to understand not only the dynamic modeling method of pipeline systems, but also the representation of dynamic parameters of SFC in different dynamic models. For analytical methods, Lin et al.[28] simplified the clamp as nonlinear spring-damping, and established a clamp-pipeline nonlinear model based on cubic stiffness. Meanwhile, the analytical solution of the nonlinear model was obtained by the multi-scale method. Chen et al.[29] studied the dynamic analysis of a liquid-filled pipeline under the condition of clamp soft nonlinear support. They simplified the clamp to a double spring-single damping model and derived the differential equation of system dynamics based on the generalized Hamilton principle. The numerical results were calculated by the Runge-Kutta method, and the approximate analytical results were obtained by the harmonic balance method. Yang et al.[30] derived a real-valued analytical formula for calculating the random stress response of a clamp-pipeline model transporting fluid based on the complex modal superposition method and random vibration theory, and the equivalent spring-damping model was used to simulate the support effect of the clamp. Zhang et al.[31] divided the L-shaped pipeline into two straight pipes and one curved pipe based on the substructure-analytical method and established a substructure-analytical dynamic model or L-shaped pipeline with multiple clamps. The clamp in the model was simulated by two groups of spring-damping elements. Dou et al.[32] established the dynamic model of a fluid-conveying pipe with flxed-flxed ends and restrained by an intermediate clamp. The clamp and the constrained pipe within the clamp width were modeled as a rigid body that had a certain width and was connected to the base by vertical and torsional springs at its ends. The influence of the clip stiffness on the natural vibration characteristics was compared, and the necessity of the integral pipe model was illustrated. For the semi-analytic models, Ma et al.[33,34] developed a new semi-analytical model for the straight pipeline segment treated by constrained layer damping and the curved pipeline segment based on the Timoshenko straight beam and curved beam theory. The clamp was equivalent to a group of spring dampers, which comprised six springs and six dampers. The dynamic equation was established by substituting in the Lagrange equation.

Further, they proposed an equivalent mechanical model to simulate the nonlinear mechanical properties of the clamp, which were expressed by nonlinear stiffness and damping with the amplitude-dependent characteristic. Meanwhile, an effective algorithm was presented for solving nonlinear dynamic equations in the frequency domain with the amplitude-dependent characteristic. Xu et al.[35] established a theoretical model by Euler-Bernoulli beam theory to describe the dynamic behavior of the pipe restrained with pipe clamps, where the pipe was excited under the combination of internal and external flows. The pipe clamp was simplified to be a support spring and a torsional spring. Chen et al.[36] introduced a novel semi-analytical dynamic model that effectively considers the influences of nonlinear clamps in parallel pipeline systems. This model simulated the vertical hysteretic restoring force of the clamp using the Bouc-Wen model. Each clamp was simplified as two sets of springs. Each set of springs was equated to two translational springs and two torsional springs along each direction. Zhang et al.[37] discretized the pipeline system into several characteristic elements, such as straight pipe, curved pipe, clamp and connecting springs, and proposed a semi-analytical modeling method for U-shaped, Z-shaped and regular spatial pipelines supported by multiple clamps. The clamp was simulated by springs. The dynamic equations of the plane and regular spatial pipeline system were obtained according to the Rayleigh-Ritz method. For models based on the finite element method, Chai et al.[38] established a finite element model (FEM) of an L-type pipeline system with clamps using Timoshenko beam theory. The clamp was divided into eight springs and dampers along the axial direction, including two linear springs, two angular springs, two linear dampers and two angular dampers. Cao et al.[39–41] proposed a nonlinear clamp model with four degrees of freedom based on the genetic algorithm and the finite element method and carried out whole finite element modeling and section modeling for the complex pipeline system supported by multiple clamps, respectively. Account for the effect of clamp width constraint, each clamp of the pipeline system was discretized into two transverse springs and two torsion springs equally along the axial direction of the pipe. Ji et al.[42,43] established two parametric order reduction FEMs for the pipeline system based on the dynamic substructure method and high-precision super element with few degrees of freedom, respectively. The spring elements are used to simulate the clamp constraint. It was assumed that the deformations of the clamp belts were equal, and the spring stiffness of the clamp support constraint was proportional to the clamping force. Ma et al.[44] proposed a FEM for nonlinear vibration analysis of the straight pipeline with a partially attached viscoelastic damping patch considering the non-uniform continuous elastic constraint of the clamp. Several spring groups were set to simulate the elastic boundary condition of clamps. Each spring group had three translational springs and two rotational springs. In addition, the transfer matrix method is also used in the study of pipeline dynamics. Guo et al.[45–47] improved the transfer matrix method and the dynamic model of a complex fluid-conveying pipeline system with series and parallel structures. And then, a dynamic model of a parallel fluid-filled pipelines-casing considering casing flexibility was developed by combining the semi-analytical method and improved transfer matrix method.

Moreover, they proposed a dynamic model of an L-shaped pipeline combining the transfer matrix method and lumped parameter method. In these models, to consider the influence of the clamp width, the clamp was equivalent to two sets of springs, consisting of three translational springs and three torsional springs.

From the above research, it can be seen that the dynamic

parameters of the clamp structure have a significant impact on the dynamic characteristics of the pipeline system. Therefore, some scholars have also conducted identification research on the dynamic parameters of the clamp. For example, Liu et al.[48] took an aviation hydraulic pipeline as the research object, and the clamp was equivalent to the combined form of the constraint point and the pipeline. The equivalent stiffness of the clamp in each direction was obtained via the finite element method. Lin et al.[49] established a nonlinear hysteretic restoring force model based on the Bouc-Wen model, and the Gamultiobj algorithm and the group search optimization (GSO) algorithm are used to fit and identify the material softening and hardening hysteresis curves, respectively.

Nonetheless, research on the identification of dynamic parameters of SFCs in aeroengine pipeline systems is still in its early stages, and corresponding parameter identification research is even rarer. In previous research on pipeline system dynamics, various modeling methods have been applied. It is worth noting that the constraint effects (stiffness and damping) of SFCs are mostly simplified into a spring-damping model in several directions. This makes the dynamic parameter identification of the SFC based on this simplified mode. Meanwhile, the mechanical structure of SFC for the aeroengine has asymmetry, which leads to the anisotropy of the dynamic parameters of the SFC in different directions. Therefore, the research on parameter identification of SFCs needs to address the problem of synchronous identification of multiple parameters. In other words, the identification model and identification algorithm need to adapt to the needs of multi-parameter identification. Additionally, experimental test data is often required as input in parameter identification.

In practical complex pipeline systems, SFCs are used in multiple positions. Using test data from actual pipeline systems as input parameters for identification will undoubtedly result in significant testing difficulty and workload. Even if it is possible to test the actual pipeline system, the use of its massive test data is still a very troublesome problem. Therefore, a simple and effective testing structure that can reflect the mechanical properties of the SFC has become the key to identifying the clamp parameters. The above factors pose a huge challenge to the research on dynamic parameter identification of SFCs.

To address these issues, an SFC-straight pipe structure for dynamic parameter identification of SFC is proposed in this paper. In this structure, one end of the straight pipe is completely fixed, and the other end is supported by an SFC. This structure can better reflect the working state of the SFC. On this basis, a dynamic model of the structure is established based on the finite element method for parameter identification of the SFC. In the FEM, the constraint effect of the SFC is simplified as two identical spring-damping groups. Considering the structural asymmetry (as shown in Fig. 2), there is a significant difference in the dynamic parameters of the SFC in the bolt direction and the opening direction. Therefore, different spring and damping parameters are set for bolt direction and opening direction in each spring-damping group. Meanwhile, using modal test data as input parameters, an identification algorithm and procedure for the dynamic parameters (stiffness and damping) of the SFC are proposed based on Pareto multi-objective genetic algorithm.

The structure of this article is organized as follows. In Section 2, the dynamic parameter identification theory of SFC is introduced, including the establishment of FEM, construction of frequency response functions (FRFs), identification algorithms and processes. In Section 3, experimental verification is conducted. Herein, parameter identification DK8 SFC is carried out, and an experimental structure is constructed that is completely supported by two SFCs to verify the accuracy of the identification results. Finally, some important conclusions are listed in Section 4.

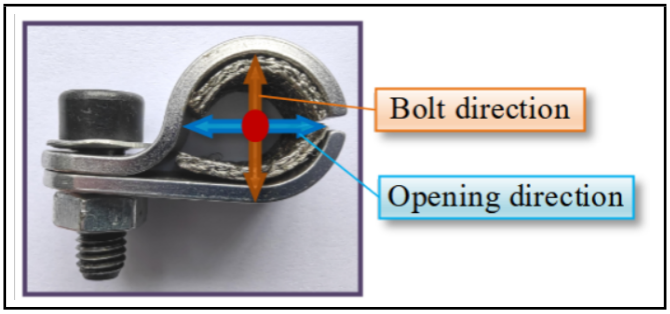

Figure 2. Bolt direction and opening direction of SFC.

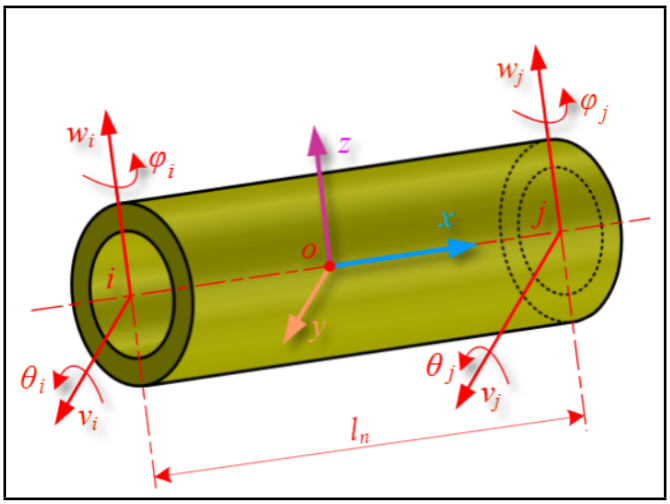

Figure 3. Timoshenko beam element.

2. IDENTIFICATION THEORY OF DYNAMIC PARAMETERS FOR SFC

2.1. Construction of FEM and FRF

Based on ignoring the axial translation and torsional deformation of the pipeline structure, Timoshenko beam elements were used for FEM. As shown in Fig. 3, the n th beam element coordinate system is $oxyz$, the subscripts i and j represent node numbers, and l_n is the length of the n th beam element, respectively. The displacement vector of the n th beam element in this coordinate system can be expressed as:

$$\delta^n = [v_i, w_i, \phi_i, \theta_i, v_j, w_j, \phi_j, \theta_j]; \tag{1}$$

The stiffness matrix of the n th beam element k_n can be expressed as where, I_y and I_z were the principal moment of inertias for the y-axis and z-axis, b_y and b_z were the shear influence coefficients on the y-axis and z-axis directions, I_x was the torsional moment of inertia for the x-axis, E was the

$$k_n = \begin{Bmatrix} \frac{EA}{l_n} & & & & & \text{Diagonal symmetric elements} & & & & & & \\ 0 & \frac{12EI_z}{l_n^3(1+b_y)} & & & & & & & & & & \\ 0 & 0 & \frac{12EI_y}{l_n^3(1+b_z)} & & & & & & & & & \\ 0 & 0 & 0 & \frac{GI_x}{l_n} & & & & & & & & \\ 0 & 0 & -\frac{6EI_y}{l_n^2(1+b_z)} & 0 & \frac{(4+b_z)EI_y}{l_n^3(1+b_z)} & & & & & & & \\ 0 & \frac{6EI_z}{l_n^2(1+b_y)} & 0 & 0 & 0 & \frac{(4+b_y)EI_z}{l_n^3(1+b_y)} & & & & & & \\ -\frac{EA}{l_n} & 0 & 0 & 0 & 0 & 0 & \frac{EA}{l_n} & & & & & \\ 0 & -\frac{12EI_z}{l_n^3(1+b_y)} & 0 & 0 & 0 & -\frac{6EI_z}{l_n^2(1+b_y)} & 0 & \frac{12EI_z}{l_n^3(1+b_y)} & & & & \\ 0 & 0 & -\frac{12EI_y}{l_n^3(1+b_z)} & 0 & \frac{6EI_y}{l_n^2(1+b_z)} & 0 & 0 & 0 & \frac{12EI_y}{l_n^3(1+b_z)} & & & \\ 0 & 0 & 0 & -\frac{GI_x}{l_n} & 0 & 0 & 0 & 0 & 0 & \frac{GI_x}{l_n} & & \\ 0 & 0 & -\frac{6EI_y}{l_n^2(1+b_z)} & 0 & \frac{(2-b_z)EI_y}{l_n(1+b_z)} & 0 & 0 & 0 & \frac{6EI_y}{l_n^2(1+b_z)} & 0 & \frac{(4+b_z)EI_y}{l_n^3(1+b_z)} & \\ 0 & \frac{6EI_z}{l_n^2(1+b_y)} & 0 & 0 & 0 & \frac{(2-b_y)EI_z}{l_n(1+b_y)} & 0 & \frac{6EI_z}{l_n^2(1+b_y)} & 0 & 0 & 0 & \frac{(4+b_y)EI_z}{l_n^3(1+b_y)} \end{Bmatrix}; \quad (2)$$

Young's modulus, A was the cross-sectional area of the beam, and G was the shear modulus.

The mass matrix of the n th beam element m_n can be expressed as

where, ρ was the material density. In addition, r_y and r_z were the rotation radii around the y-axis and z-axis, $A_z = A(r_z, b_y)$, $A_y = A(r_y, b_z)$, $B_z = B(r_z, b_y)$, $B_y = B(r_y, b_z)$, $C_z = C(r_z, b_y)$, $C_y = C(r_y, b_z)$, $D_z = D(r_z, b_y)$, $D_y = D(r_y, b_z)$, $E_z = E(r_z, b_y)$, $E_y = E(r_y, b_z)$, $F_z = F(r_z, b_y)$, $F_y = F(r_y, b_z)$.

r_y and r_z can be calculated using the following formulas.

$$r_y = \sqrt{\frac{I_y}{A}}; \quad (4a)$$

$$r_z = \sqrt{\frac{I_z}{A}}; \quad (4b)$$

The expressions of A_z, A_y, B_z, B_y, C_z, C_y, D_z, D_y, E_z, E_y, F_z and F_y were as follows

$$A(r,b) = \frac{\frac{13}{35} + \frac{7}{10}b + \frac{1}{3}b^2 + \frac{6}{5}(\frac{r}{l_n})^2}{(1+b)^2}; \quad (5a)$$

$$B(r,b) = \frac{\frac{9}{70} + \frac{3}{10}b + \frac{1}{6}b^2 + \frac{6}{5}(\frac{r}{l_n})^2}{(1+b)^2}; \quad (5b)$$

$$C(r,b) = \frac{\left[\frac{11}{210} + \frac{11}{120}b + \frac{1}{24}b^2 + (\frac{1}{10} - \frac{1}{2}b)(\frac{r}{l_n})^2\right]l_n}{(1+b)^2}; \quad (5c)$$

$$D(r,b) = \frac{\left[\frac{3}{420} + \frac{3}{40}b + \frac{1}{24}b^2 - (\frac{1}{10} - \frac{1}{2}b)(\frac{r}{l_n})^2\right]l_n}{(1+b)^2}; \quad (5d)$$

$$E(r,b) = \frac{\left[\frac{1}{105} + \frac{1}{60}b + \frac{1}{120}b^2 - (\frac{2}{15} + \frac{1}{6}b + \frac{1}{3}b^2)(\frac{r}{l_n})^2\right]l_n}{(1+b)^2}; \quad (5e)$$

$$F(r,b) = \frac{\left[\frac{1}{140} + \frac{1}{60}b + \frac{1}{120}b^2 - (\frac{1}{30} + \frac{1}{6}b + \frac{1}{6}b^2)(\frac{r}{l_n})^2\right]l_n}{(1+b)^2}; \quad (5f)$$

To achieve parameter identification of SFC, the SFC-straight pipeline structure is designed as shown in Fig. 4. In this structure, the D_1 end of the pipeline was completely fixed, and the D_2 end was fixed with an SFC. In the FEM, the SFC was simulated using a spring-damping element. The position points of d_1 and d_2 represented the constraint position of the SFC. The clamp was equivalent to two linear springs connected in parallel to the pipeline. k_z and k_y represented the radial stiffness of the clamp, $k_{\theta z}$ and $k_{\theta y}$ represented the torsional stiffness of the clamp, c_z and c_y represent radial support damping. The damping of the clamp in the torsion direction is not considered. In the Fig. 4, the stiffness matrix and damping matrix of SFC (K_{cl}, C_{cl}) are

$$K_{cl} = \begin{bmatrix} K_y & & & \\ & K_z & & \\ & & K_{\theta y} & \\ & & & K_{\theta z} \end{bmatrix}; \quad (6)$$

$$C_{cl} = \begin{bmatrix} C_y & 0 \\ 0 & C_z \end{bmatrix}. \quad (7)$$

The stiffness matrix and damping matrix of the SFC-straight pipe structure (K, C) can be expressed as

$$K = K_{cl} + K_{pi}; \quad (8)$$

$$C = C_{cl} + C_{pi}; \quad (9)$$

where, K_{pi} and C_{pi} were the stiffness matrix and damping matrix of the straight pipe structure, respectively.

Among them, the damping matrix of the straight pipe C_{pi} was simulated using Rayleigh damping, that was, $C_{pi} = \alpha M + \beta K$. α and β were Rayleigh damping coefficients, and can be obtained from following formula.

$$\alpha = \frac{2\bar{\omega_t}\bar{\omega_p}(\zeta_t\bar{\omega_p} - \zeta_p\bar{\omega_t})}{\bar{\omega_p}^2 - \bar{\omega_t}^2}; \quad (10a)$$

$$\beta = \frac{2(\zeta_p\bar{\omega_p} - \zeta_t\bar{\omega_t})}{\bar{\omega_p}^2 - \bar{\omega_t}^2}; \quad (10b)$$

where, ζ_t and ζ_t were structural damping ratios of the t th order and u th order, $\bar{\omega_t}$ and $\bar{\omega_p}$ were natural circular frequencies of the t th order and p th order (unit: rad/s). The orders (t and p) were determined based on the minimum and maximum values of the analysis range of interest. For the system studied in this paper, 1 st and 20 th orders are selected, i.e. $t = 1, p = 20$.

The straight pipe was divided into N elements. The stiffness and damping matrices of the clamp and pipe body were assembled. The stiffness and damping matrices of the SFC-straight

$$m_n = \rho A l_n \begin{Bmatrix} \frac{1}{3} & & & & & & & & & & \\ 0 & A_z & & & & & & & & & \\ 0 & 0 & A_y & & & & & & & & \\ 0 & 0 & 0 & \frac{I_x}{3A} & & & & & & & \\ 0 & 0 & -C_y & 0 & E_y & & & & & & \\ 0 & C_z & 0 & 0 & 0 & E_z & & & & & \\ \frac{1}{6} & 0 & 0 & 0 & 0 & 0 & \frac{1}{3} & & & & \\ 0 & B_z & 0 & 0 & 0 & D_z & 0 & A_z & & & \\ 0 & 0 & B_y & 0 & -D_y & 0 & 0 & 0 & A_y & & \\ 0 & 0 & 0 & \frac{I_x}{6A} & 0 & 0 & 0 & 0 & 0 & \frac{I_x}{3A} & \\ 0 & 0 & D_y & 0 & F_y & 0 & 0 & 0 & -C_y & 0 & E_y \\ 0 & -D_z & 0 & 0 & 0 & F_z & 0 & -C_z & 0 & 0 & 0 & E_z \end{Bmatrix}; \quad (3)$$

Diagonal symmetric elements

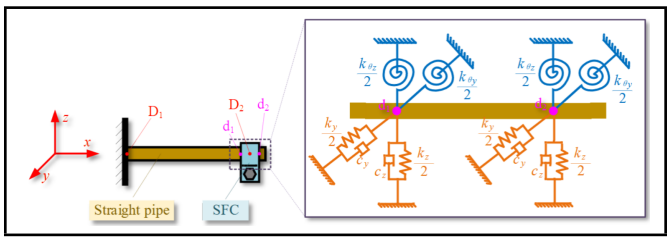

Figure 4. SFC-straight pipeline structure.

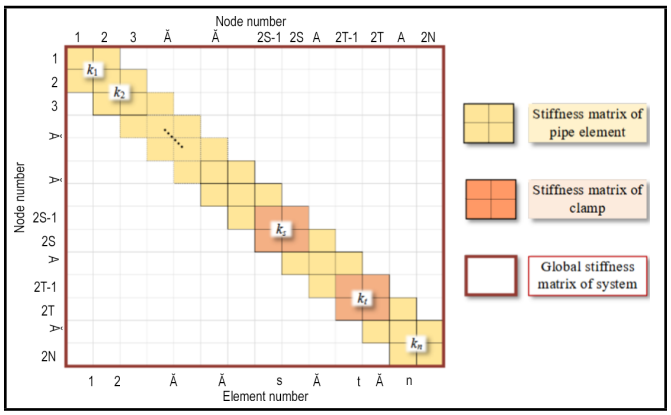

Figure 5. The system stiffness matrix set of SFC-straight pipe structure.

pipe system were obtained through this method. The assembly method is shown in Fig. 5 and Fig. 6.

From the above formulas, the dynamic equation of the SFC-straight pipe structure can be obtained

$$M\ddot{X} + C\dot{X} + KX = F; \quad (11)$$

where, M was the mass matrix of the SFC-straight pipe structure, which was obtained by adding the clamp mass as a concentrated mass to the mass matrix of the pipe.

The displacement FRF of the SFC-straight pipe structure was

$$H_s(\omega) = \sum_{r=1}^{n} \frac{\phi_r \phi_r^T}{\omega_r^2 + 2i\zeta_r\omega_r\omega - \omega^2}; \quad (12)$$

where, ω was the external excitation frequency, ω_r was the r th order natural frequency of the system, ζ_r was the r th modal damping ratio of the system, n was the number of calculated modes, ϕ was a vibration mode matrix composed of n orders vibration mode vectors.

In this paper, the acceleration FRF was used for damping identification. Therefore, Eq. (12) was converted to Eq. (13), and the real part value of Eq. (13) is taken as the calculation result.

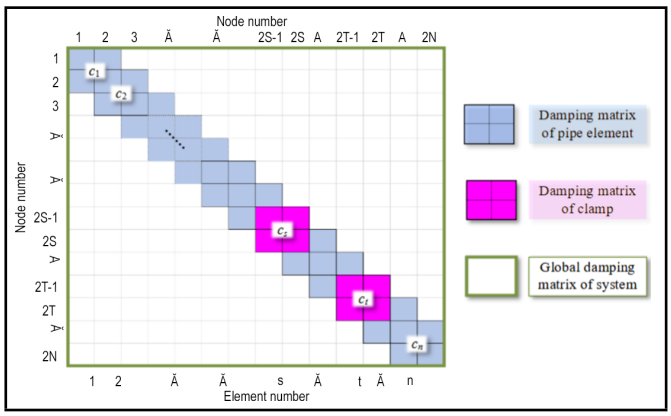

Figure 6. The system damping matrix set of SFC-straight pipe structure.

$$H_s(\omega) = \sum_{r=1}^{n} \frac{-\omega^2 \phi_r \phi_r^T}{\omega_r^2 + 2i\zeta_r\omega_r\omega - \omega^2}; \quad (13)$$

2.2. Identification Algorithm

The optimization process of Pareto genetic algorithm can be described as follows

$$\min[f_1(\bar{x}), f_2(\bar{x}), \cdots f_m(\bar{x})]; \quad (14a)$$

$$s.t \begin{cases} lb \le \bar{x} \le ub \\ Aeq * \bar{x} = beq \\ A * \bar{x} \le b \end{cases}; \quad (14b)$$

where, $f_i(x)$ was the objective function to be optimized, and $\bar{x}$ was the variable to be optimized. Constraint: lb and ub were the upper and lower limits of $\bar{x}$, Aeq and beq constituted the linear equality constraint of $\bar{x}$, A and b constituted the linear inequality constraint of $\bar{x}$.

2.2.1. Identification algorithm for clamp stiffness

The natural frequencies of each order for the system can be obtained separately through modal testing and simulation analysis (based on the FEM proposed in Section 2.1). The objective function of Pareto algorithm is constructed based on the error between the test results and simulation results of the natural frequency, which can be expressed as

$$\min\{\frac{|f_1 - f_{m1}|}{f_1}, \frac{|f_2 - f_{m2}|}{f_2}, \cdots \frac{|f_i - f_{mi}|}{f_i}\}; \quad (15)$$

where, f_i and $f_m i$ were the natural frequencies obtained from the modal testing and simulation. The range of stiffness K is

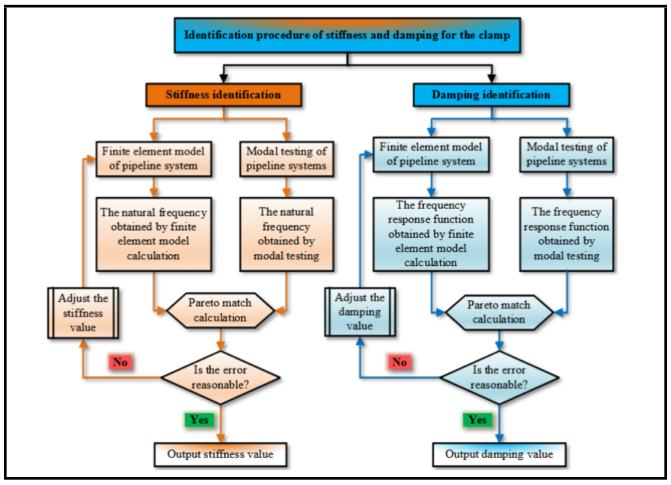

Figure 7. Identification procedure for stiffness and damping of clamp.

set as a constraint condition $\bar{x}$, that is

$$lb \leq K \leq ub; \tag{16}$$

where, the values of lb and ub were determined by static experiments.

2.2.2. Identification algorithm for clamp damping

Similarly, the FRFs corresponding to each order of natural frequencies can be obtained through modal testing and simulation analysis. Based on the error between the test results and simulation results of the FRFs, the Pareto algorithm objective function is constructed as follows

$$\min\{\frac{|H_1 - H_{m1}|}{H_1}, \frac{|H_2 - H_{m2}|}{H_2}, \cdots \frac{|H_i - H_{mi}|}{H_i}\}; \tag{17}$$

where, H_i and H_{mi} were the FRFs obtained from the modal testing and simulation. The ranges of the damping c_j and structural damping ratios ζ_1 and ζ_2 in Rayleigh damping were set as constraint conditions $\bar{x}$, that is

$$lb_1 \leq c_j \leq ub_1; \tag{18a}$$

$$lb_2 \leq \zeta_1 \text{or} \zeta_2 \leq ub_2; \tag{18b}$$

where, c_j was the damping in the $j(x, y, z)$ direction, lb_1, ub_1, lb_2 and ub_2 are determined by static tests.

2.3. Identification Procedure

The natural frequencies of the pipeline system are directly affected by the support stiffness of the clamp, and the FRF of the pipeline system is directly affected by the clamp damping. Therefore, the stiffness and damping of the clamp can be directly identified through the natural frequencies, and FRF obtained through modal testing. The identification procedure for the stiffness and damping of clamp is shown in Fig. 7.

3. EXPERIMENTAL VERIFICATION

To accurately verify the reliability of the identification algorithm, two experimental structures are set up:

1. A single straight pipe with one end fixed and the other end supported with an SFC.
2. A single straight pipe supported with two SFCs.

Firstly, the stiffness and damping of the SFC are identified using the first experimental structure, and then the identification results are substituted into the second experimental structure for verification.

The DK8 SFCs and a 400 mm straight steel pipe were used in the experiment, and the geometric and material parameters of the pipe body are shown in Tab. 1.

Table 1. Material and geometric parameters of pipe.

Elastic modulus (GPa)	Density (kg/m^3)	Poisson's ratio	Length (mm)	Outside diameter (mm)	Inside diameter (mm)
190	7850	0.3	400	8	6.4

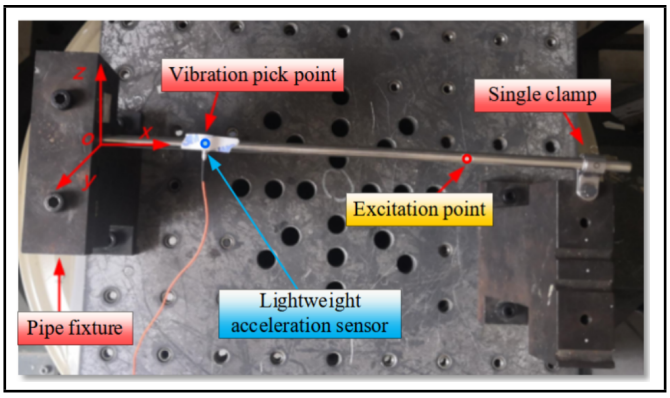

Figure 8. Testing system for identifying the stiffness and damping of DK8 SFC.

3.1. Identification of Stiffness and Damping of DK8 SFC

The layout of the testing system used to identify the stiffness and damping of the clamp is shown in Fig. 7. One end of the straight pipe was completely fixed by a fixture, and the other end was fixed by an SFC. The SFC was fixed by a bolt, and the bolt tightening torque is 7 N·m. Here, the impact method was used for modal testing. The excitation point and pickup point of vibration are shown in Fig. 8. The coordinates of the excitation point was (284 mm, 0, 0), and the pickup point of vibration was (110 mm, 0, 0). A PCB lightweight unidirectional acceleration sensor was used to capture the vibration. The natural frequency and FRF of the system can be obtained through modal testing. Then, the FEM of the experimental testing structure needs to be established. Except for the fixed support area on the left side, the effective length of the straight pipe is 320 mm.

3.1.1. Stiffness identification

In the testing modal data, the 3 orders natural frequencies dominated by the y-direction stiffness of the clamp were selected for identification of the y-direction stiffness of the clamp, and the 3 orders natural frequencies dominated by the z-direction stiffness of the clamp were selected for identification of the z-direction stiffness of the clamp. According to the stiffness identification algorithm proposed in Section 2.2, the constraint condition is set to the magnitude of the stiffness in the four degrees of freedom directions of the clamp, and the range of values is given by the static experiment. The con-

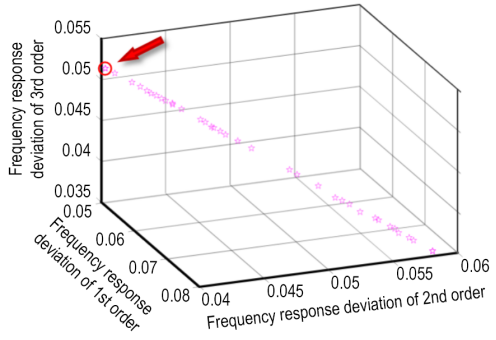

(a) Optimization results with 1st-3rd orders

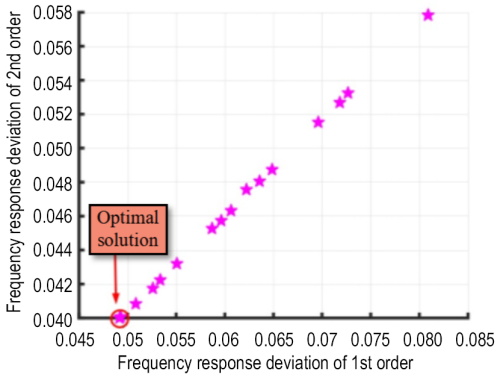

(b) Optimization results with 1st and 2nd orders

Figure 9. z-direction stiffness optimization results SFC.

straints of stiffness identification are represented as

$$\begin{cases} 5.9 \times 10^6 \leq K_y \leq 8.8 \times 10^6 \\ 3.4 \times 10^6 \leq K_z \leq 4.9 \times 10^6 \\ 31 \leq K_{\theta y} \leq 42 \\ 17 \leq K_{\theta z} \leq 39 \end{cases} \tag{19}$$

; The population size was set to 100, and the number of iterations was set to 100. The optimization results are shown in Fig. 9 (taking the calculation of -direction stiffness as an example). The optimization results with the 1st-3rd natural frequencies as the optimization objective are shown in Fig. 9 (a), and the optimization results with the 1 st and 2 nd natural frequencies as the optimization objective are shown in Fig. 9 (b). The 1 st and 2 nd natural frequencies can simultaneously achieve the minimum error, which is the position indicated in Fig. 9 (b). However, the error of the 3 rd natural frequency is not the minimum. Therefore, when selecting the optimization results, the optimization objective of interest can be considered. For example, this study focuses more on natural frequencies below 1000 Hz, so the minimum error of the 1 st and 2 nd natural frequencies is selected as the final optimization result. The optimal solution can be obtained from Fig. 9, and the optimization results of the clamp stiffness in the y and z directions are listed in Tab. 2 and Tab. 3. According to the frequency data in Tab. 2 and Tab. 3, the frequency errors ($|f_i - f_{mi}|/f_i$) are further calculated, and the calculation results are shown in Fig. 10. For the experimental frequency and simulation frequency of y-direction stiffness identification, the maximum frequency error is 0.675 %, and the average frequency error is 0.355 %. For the experimental frequency and simulation frequency of -direction stiffness identification, the maximum frequency error is 5.156 %, and the average frequency error is 4.691 %. This frequency error level meets the actual needs of engineering.

Table 2. Optimization results of y-direction stiffness of DK8 single clamp.

Order	Experimental frequency f_i	Calculated frequency f_{mi}	Identification result
1	337.500 Hz	336.721 Hz	K_y=8669322 N/m
2	946.875 Hz	948.390 Hz	K_z=4158579 N/m
3	1881.250 Hz	1855.664 Hz	$K_{\theta}y$=35.02 N/rad $K_{\theta}z$=36.96 N/rad

Table 3. Optimization results of z-direction stiffness of DK8 single clamp.

Order	Experimental frequency f_i	Calculated frequency f_{mi}	Identification result
1	337.500 Hz	320.903 Hz	K_y=7729826 N/m
2	959.375 Hz	921.000 Hz	K_z=4894975 N/m
3	1737.500 Hz	1827.082 Hz	$K_{\theta}y$=42 N/rad $K_{\theta}z$=32.73 N/rad

3.1.2. Damping identification

The identification results of the clamp stiffness are input into the identification model. Meanwhile, the FRF values of 2 orders dominated by y-direction damping were selected to identify the y-direction damping of the clamp, and the FRF values of 2 orders dominated by z-direction damping were selected to identify the z-direction damping of the clamp. The objective function was constructed using the corresponding acceleration FRF. Based on the damping identification algorithm proposed in Section 2.2, the damping (c_y, c_z) and Rayleigh damping ratios (ζ_1, ζ_2) in the y-direction and z-direction were set as constraint conditions, and their range of values is given by static experiments. The constraints of damping identification are represented as

$$\begin{cases} 0 \leq \zeta_1 \leq 1 \\ 0 \leq \zeta_2 \leq 1 \\ 6 \leq c_y \leq 50 \\ 3 \leq c_z \leq 32 \end{cases} . \tag{20}$$

The population size is set to 30 and the number of iterations is set to 100. The optimization results are shown in Fig. 10 (To save paper space, the calculation of z-direction damping with 1 st and 2 nd orders is taken as an example). From Fig. 11, it can be seen that the optimal solution occurs when the FRF error of the 1 st and 2 nd orders is the minimum, and the damping and structural damping ratios in the y-direction and z-direction can be obtained. The identification results are listed in Tab. 4 and Tab. 5. Similarly, the frequency response errors ($|H_i - H_{mi}|/H_i$) are calculated based on the FRF values in Tab. 4 and Tab. 5, and the calculation results are shown in Fig. 12. For experimental frequency response and simulation frequency response of y-direction damping identification, the maximum frequency response error is 1.151 %, and the average frequency response error is 1.089 %. For experimental frequency response and simulation frequency response of z-direction damping identification, the maximum frequency response error is 0.013 %, and the average frequency response

Table 4. Optimization results of y-direction damping of DK8 single clamp.

Order	Experimental frequency response H_i[(m/s^2)/N]	Simulation frequency response H_{mi}[(m/s^2)/N]	Identification result
1	283.12	286.37	ζ_1 = 0.023 ζ_2 = 0.032 c_y = 15.77
2	1379.77	1365.60	

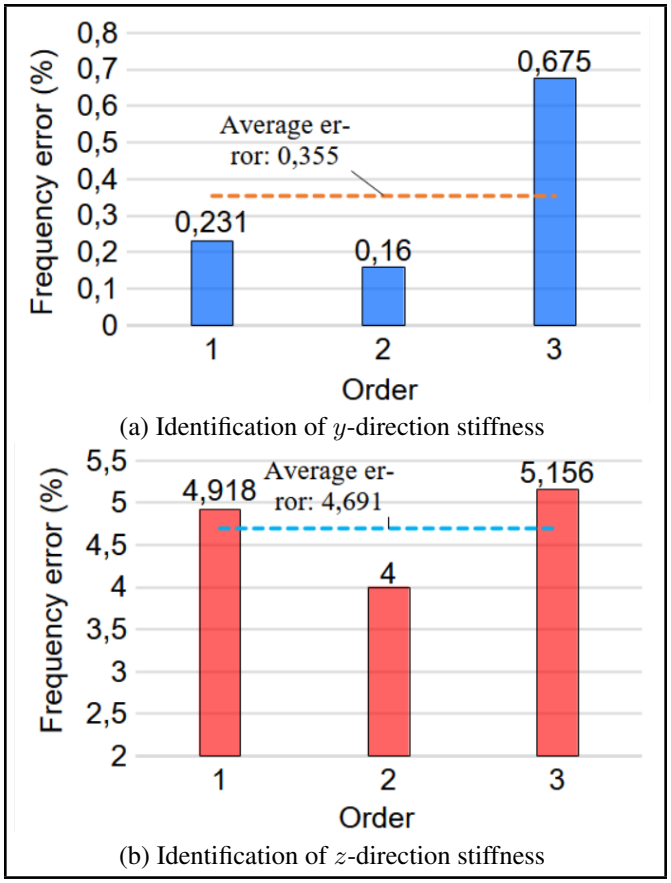

Figure 10. Frequency error in stiffness identification of y-direction and z-direction.

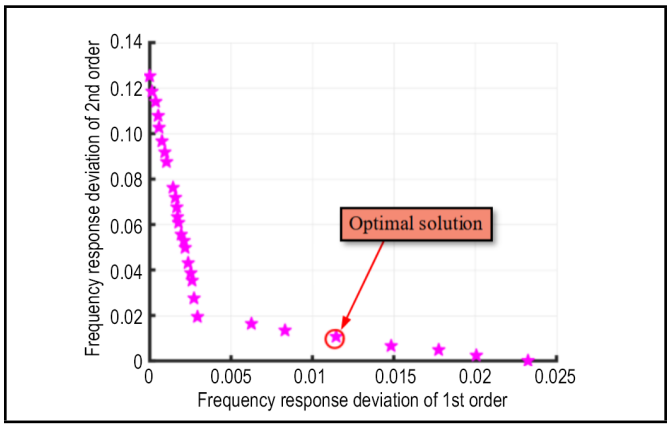

Figure 11. z-direction damping optimization results with 1 st and 2 nd orders.

Table 5. Optimization results of z-direction damping of DK8 single clamp.

Order	Experimental frequency response H_i[(m/s^2)/N]	Simulation frequency response H_{mi}[(m/s^2)/N]	Identification result
1	925.52	925.60	$\zeta_1 = 0.006$ $\zeta_2 = 0.11$ $c_y = 15.97$
2	1180.11	1179.96	

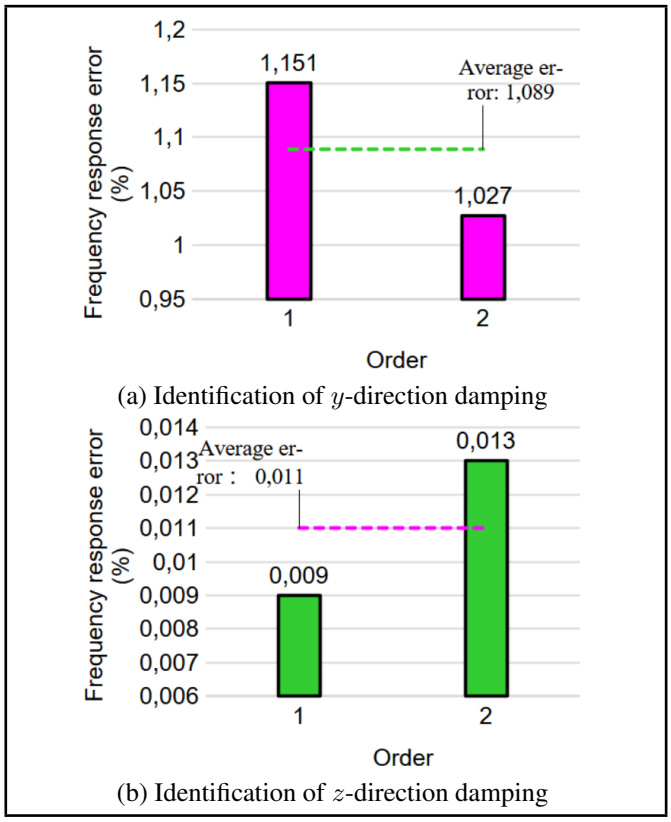

Figure 12. Frequency error in damping identification of y-direction and z-direction.

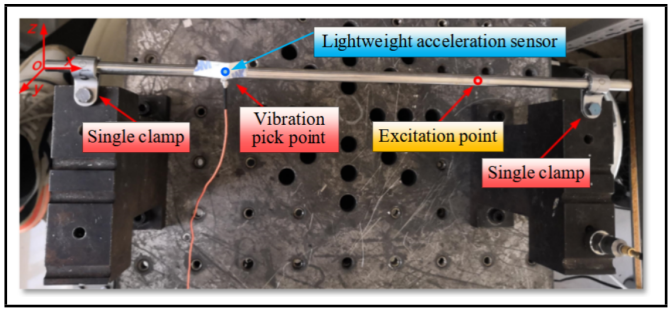

Figure 13. Experimental testing system for verifying identification results.

error is 0.011 %. This frequency response error level also meets the actual engineering needs.

3.2. Verification of Identification Results

To verify the correctness of the identification results in Section 3.1, an experimental system was built with a straight pipe supported by two DK8 single clamps. As shown in Fig. 13, the 2 ends of the straight pipe were fixed to the experimental bench using two single clamp bolts. Similarly, the impact method was selected for modal testing to obtain the natural frequencies and FRF of the experimental structure. The bolt torque for fixing the clamp is 7 Nm, which was the same as the clamp bolt torque for the experimental structure in Section 3.1. Similarly, a FEM of the experimental structure needs to be established. In this experimental structure, the effective length of the straight tube was 400 mm. Based on the FEM in Section 2.1, the pipe body was divided into 80 elements and 81 nodes. The 2 clamps were simplified into four support points corresponding to nodes 4, 7, and 74, 77 of the pipe body, and the concentrated mass effect of the clamps was considered. The

Table 6. Experimental and simulated natural frequencies of the 1st-3th orders in the y-direction and z-direction.

Order	y-direction		z-direction	
	Experimental frequency f_i [Hz]	Simulated frequency f_{mi} [Hz]	Experimental frequency f_i [Hz]	Simulated frequency f_{mi} [Hz]
1	281.25	272.10	268.75	246.4
2	803.13	783.75	756.25	736.53
3	1615.63	1553.58	1487.5	1475.74

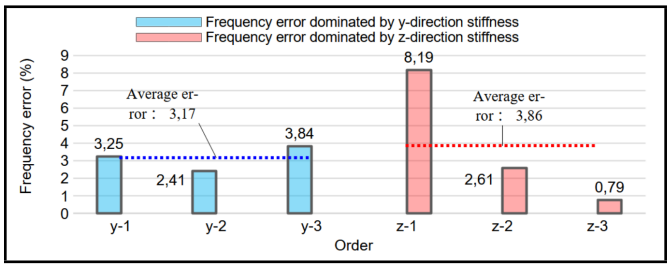

Figure 14. Frequency error for verification of y-direction stiffness and z-direction stiffness.

identification results of clamp stiffness and damping in Section 3.1 are input into the FEM for modal analysis. 3 orders of experimental and simulated natural frequencies dominated by stiffness of the y-direction and z-direction were selected for comparison (as shown in Tab. 6).

Furthermore, the frequency errors ($|f_i - f_{mi}|/f_i$) were calculated, and the calculation results are shown in Fig. 14. For the identification stiffness of y-direction, the maximum frequency error is 3.84 %, and the average frequency error is 3.17 %. For identification stiffness of z-direction, the maximum frequency error is 8.19 %, and the average frequency error is 3.86 %. The comprehensive average frequency error in both directions is 3.52 %. The results of the above comparison demonstrate that the experimental frequencies and simulation frequencies have good consistency, and the effectiveness of the identification method for identifying the stiffness of clamps is verified.

After verifying the correctness of the stiffness identification results, the damping coefficients identified in Section 3.1 are incorporated into the FEM of the pipeline structure with 2 single clamps. Similarly, the FRFs of two orders dominated by y-direction damping and z-direction damping are selected as optimization objectives. The objective function is set to the acceleration FRF error of pipeline structure with 2 single clamps. The constraint parameters are the damping ratios of this structure ζ_1 and ζ_2, and the constraint ranges are represented as follows.

$$\begin{cases} 0 \le \zeta_1 \le 1 \\ 0 \le \zeta_2 \le 1 \end{cases} . \tag{21}$$

Herein, the population size is set to 30 and the number of iterations is set to 100. The calculation results are shown in Fig. 15. As shown in Fig. 15, the optimal solution is the case where the FRF deviation of the two orders is the smallest. Therefore, the damping ratios in the y-direction and the z-direction listed in Tab. 7 and Tab. 8 can be obtained. Furthermore, the FRF errors ($|H_i - H_{mi}|/H_i$) were calculated, and the calculation results are shown in Fig. 16. For the identification damping of y-direction, the maximum FRF error is 0.264 %, and the average FRF error is 0.177 %. For identification damping of z-direction, the maximum FRF error is

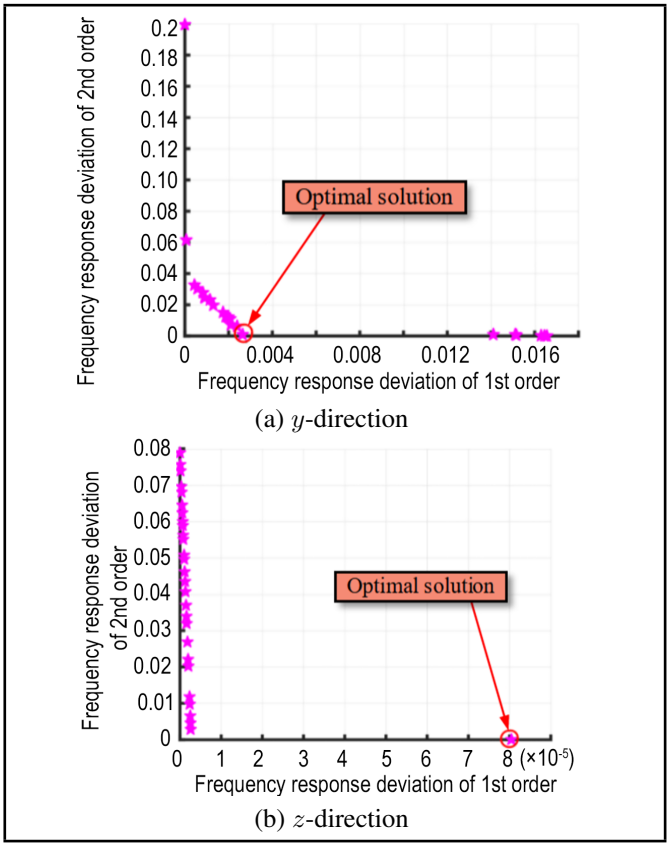

Figure 15. Calculation results of Damping ratios ζ_1 and ζ_2 .

Table 7. Calculation results of y-direction damping.

Order	Experimental frequency response H_i[(m/s^2)/N]	Simulation frequency response H_i[(m/s^2)/N]	Calculation result
1	387.17	388.20	ζ_1 = 0.028
2	1415.52	1416.79	ζ_1 = 0.041

0.008 %, and the average FRF error is 0.005 %. The comprehensive average error of FRF in both directions is 0.091 %. The above comparison results demonstrate that the experimental and simulation FRF values have good consistency, and the effectiveness of the identification method proposed in this paper for identifying the damping of clamps is verified. Next, the FRF curves of the test and simulation were compared. As shown in Fig. 17, the FRF curve of 2 orders dominated by damping in the y-direction are compared. The FRF curves of the test and simulation are in good agreement, which further verifies the effectiveness of the identification method proposed in this paper.

4. CONCLUSIONS

In this paper, an experimental structure for identifying the stiffness and damping parameters of an SFC is proposed. Meanwhile, an identification model for the clamp stiffness pa-

Table 8. Calculation results of z-direction damping.

Order	Experimental frequency response H_i[(m/s^2)/N]	Simulation frequency response H_i[(m/s^2)/N]	Calculation result
1	927.41	927.48	ζ_1 = 0.0093
2	2295.00	2294.96	ζ_1 = 0.027

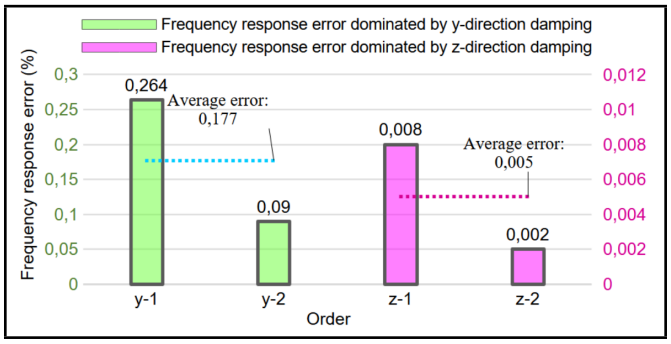

Figure 16. FRF error for verification of y-direction damping and z-direction damping.

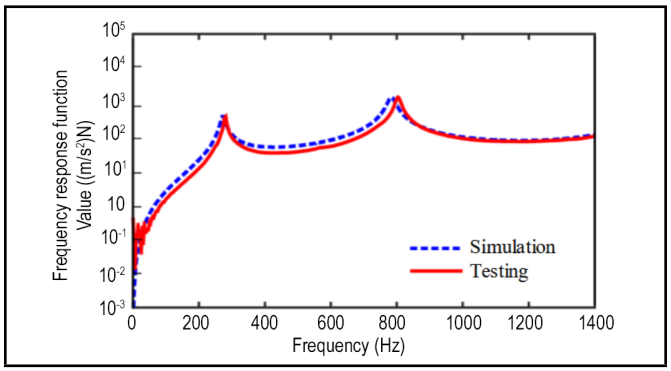

Figure 17. omparison of FRF curves dominated by damping in the y-direction.

rameters is established, and a parameter identification procedure based on modal test data is proposed. Furthermore, experimental research is conducted, and the following conclusions are obtained.

1. The structure of a straight pipe with one end fixed and one end supported by a clamp proposed in this paper is feasible for identifying the stiffness and damping parameters in the bolt direction and opening direction of a single clamp.

2. The parameter identification model for the SFC based on Timoshenko theory and simplified clamp support structure is effective, and the proposed identification procedure for SFC parameters based on modal testing and Pareto algorithm has good identification results.

3. Taking DK8 single coupling clamp as the research object, a pipeline structure supported by two clamps is constructed. The parameter identification results of the clamp are incorporated into the dynamic model of this structure for simulation analysis, and the simulation and experimental results are compared. The comparative average frequency error in both directions is 3.52 %, and the comparative average error of FRF in both directions is 0.091 %. The comparison results show that the frequency and FRF of simulation and experiment are highly consistent, which further verifies the rationality of the identification method.

4. The parameter identification algorithm based on multi-objective optimization proposed in this paper essentially linearizes the nonlinear mechanical characteristics of the clamping force locally. The frequency range included in the objective function is too large, which will affect the identification accuracy. Setting the objective function based on the frequency range of interest can achieve good identification accuracy.

ACKNOWLEDGEMENTS

This work was supported by the National Natural Science Foundation of China (52375085), the National Science and Technology Major Project (J2019-I-0008-0008) , the Fundamental Research Funds for the Central Universities of China (N2203006 and N2303018) and Guangdong Basic and Applied Basic Research Foundation (2024A1515010675).

REFERENCES

[1] Zhang, X. T. and Liu, W., The effect of pipeline layout parameters on mode and dynamic stress of "airframe clamps-pipeline" structure, *Multidiscipline Modeling in Materials and Structures*, **16**(2), 373-389, (2020) https://doi.org/10.1108/MMMS-05-2019-0106

[2] Mao, G. T., Hong, L., Wang, J. L., Wang, Z. H., Dhupia, J. S. and Liu, M. Y., Diagnosis of clamp looseness for hydraulic pipelines using fiber-Bragg-grating-based strain measurement: A feasibility study, *International Conference on Advanced Intelligent Mechatronics, IEEE*, 679-684, (2019) https://doi.org/10.1109/aim.2019.8868556

[3] Liu, Z. H., Shan, Z. C., Zhang, X. F. and Ma, H., Uncertain frequency response analysis of clamp-pipe systems via the coordinate transformed polynomial chaos expansion, *International Journal of Pressure Vessels and Piping*, **199**, 104720, (2022) https://doi.org/10.1016/j.ijpvp.2022.104720

[4] Xiao, N., Lu, L., Wei, Q. and Yang, F., A novel looseness detection method for hydraulic pipeline clamp based on statistical analysis, *2018 9th International Conference on Mechanical and Aerospace Engineering (ICMAE)*, 347-351, (2018) https://doi.org/10.1109/ICMAE.2018.8467655

[5] Yang, Y. B. and Zhang, Y. H., Random vibration response of three-dimensional multi-span hydraulic pipeline system with multipoint base excitations, *Thin-Walled Structures*, **166**, 108124, (2021). https://doi.org/10.1016/j.tws.2021.108124

[6] Yang, F., Jiang, X. M., Wei, Q., Lu, L., Xiao, N. and Wang, Z. C., Clamps looseness detection of hydraulic pipelines based on convolutional neural network, *CSAA/IET International Conference on Aircraft Utility Systems*, 764-768, (2018). https://doi.org/10.1049/cp.2018.0310

[7] Zhang, X. T., Liu, W., Zhang, Y. M. and Zhao, Y. J., Experimental investigation and optimization design of multi-support pipeline system, *Chinese Journal of Mechanical Engineering*, **34**(1), 10, (2021). https://doi.org/10.1186/s10033-020-00530-7

[8] Huang, Y. F., Wei, Q., Li, X. W., Shi, T., Zhang, J. X. and Zhu, A. D., Identification of clamps looseness based on multi-scale convolutional neural network for hydraulic

pipelines, *The 2019 4th International Conference*, 16-20, (2019). https://doi.org/10.1145/3351180.3351211

[9] Zhang, D. C., Juan, M. X., Zhang, Z. Y., Gao, P. X., Jin, J., Wang, J. J. and Yu, T., A dynamic modeling approach for vibration analysis of hydraulic pipeline system with pipe fitting, *Applied Acoustics*, **197**, 108952, (2022). https://doi.org/10.1016/j.apacoust.2022.108952

[10] Zhermolenko, V. N., Application of the method of extremal deviations to studying forced parametric bending vibrations of the pipeline, *Automation and Remote Control*, **69**, 1454-1474, (2008). https://doi.org/10.1134/S0005117908090026

[11] Hu, Z. P., Ren, X., Wang, Q. Y., Wang, R. and Pen, R., Analytical method for the mechanical response of buried pipeline under the action of strike-slip faulting, *Underground Space*, **7**, 268-277, (2022). https://doi.org/10.1016/j.undsp.2021.08.003

[12] Giacobbi, D. B., Rinaldi, S., Semler, C. and Paidoussis, M., The dynamics of a cantilevered pipe aspirating fluid studied by experimental, numerical and analytical methods, *Journal of Fluids and Structures*, **30**, 73-96, (2012). https://doi.org/10.1016/j.jfluidstructs.2011.11.011

[13] Saberi, M., Behnamfar, F. and Vafaeian, M., A semi-analytical model for estimating seismic behavior of buried steel pipes at bend point under propagating waves, *Bulletin of Earthquake Engineering*, **11**, 1373-1402, (2013). https://doi.org/10.1007/s10518-013-9430-y

[14] Huang, X. G. and Xu, J. Q., Numerical procedure for static and dynamic analysis of fluid-conveying submarine pipeline span on linear elastic seabed, *Journal of Shanghai Jiaotong University (Science)*, **15**, 719-725, (2010). https://doi.org/10.1007/s12204-010-1075-2

[15] Zhang, X., Cao, Y. G., Zhen, Y., Ren, C. Y., Wang, Z. Z., Huang, D. and Jiang, K., Method of strain analysis of pipelines under landslides: An improved semi-analytical method for softening bending moment-curvature, *Thin-Walled Structures*, **192**, 111222, (2023). https://doi.org/10.1016/j.tws.2023.111222

[16] Bezborodov, S. A. and Ulanov, A. M., Calculation of vibration of pipeline bundle with damping support made of MR material, *Procedia Engineering*, **176**, 169-174, (2017). https://doi.org/10.1016/j.proeng.2017.02.285

[17] Yang, Y. B., Qin, Z. H. and Zhang, Y. H., Random response analysis of hydraulic pipeline systems under fluid fluctuation and base motion, *Mechanical Systems and Signal Processing*, **186**, 109905, (2023). https://doi.org/10.1016/j.ymssp.2022.109905

[18] Xia, X. Y., Wu, D., Yang, F., Hu, M. W., Ma, L. H., Li, M. K., Dong, X. Y. and Duan, Z. Y., Early underground pipeline collapse detection and optimization based on water hammer vibration signal, *International Journal of Pressure Vessels and Piping*, **206**, 105045, (2023). https://doi.org/10.1016/j.ijpvp.2023.105045

[19] Zhang, X. T., Liu, W., Zhang, Y. M. and Zhao, Y. J., Experimental investigation and optimization design of multi-support pipeline system, *Chinese Journal of Mechanical Engineering*, **34**, 10, (2021). https://doi.org/10.1186/s10033-020-00530-7

[20] Tang, Z. C., Lu, Z. Z., Li, D. W. and Zhang, F., Optimal design of the positions of the hoops for a hydraulic pipelines system, *Nuclear Engineering and Design*, **241**, 4840-4855, (2011). https://doi.org/10.1016/j.nucengdes.2011.08.058

[21] Han, S. R. and Cho, J. R., Investigation of vibration damping characteristics of automotive air conditioning pipeline systems, *International Journal of Precision Engineering and Manufacturing*, **17**(2), 209-215, (2016). https://doi.org/10.1007/s12541-016-0027-7

[22] Ji, W. H., Sun, W., Ma, H. W. and Li, J. X., Dynamic modeling and analysis of fluid-delivering cracked pipeline considering breathing effect, *International Journal of Mechanical Sciences*, **264**, 108805, (2023). https://doi.org/10.1016/j.ijmecsci.2023.108805

[23] Liu, G. M., Li, S. J., Li, Y. and Chen, H., Vibration analysis of pipelines with arbitrary branches by absorbing transfer matrix method, *Journal of Sound and Vibration*, **332**, 6519-6536, (2013). https://doi.org/10.1016/j.jsv.2013.06.019

[24] Mikota, G., Low Frequency Correction of a Multi-degrees-of-freedom Model for Hydraulic Pipeline Systems, *International Federation of Automatic Control*, **48**(1), 435-440, (2015). https://doi.org/10.1016/j.ifacol.2015.05.081

[25] Batura, A., Novikov, A., Pashchenko, A. and Dubyk, Y., An application of the transfer matrix approach for a dynamic analysis of complex spatial pipelines, *Nuclear Engineering and Design*, **349**, 174-182, (2019). https://doi.org/10.1016/j.nucengdes.2019.04.035

[26] Tuozzo, D. M., Silva, O. M., Kulakauskas, L. V. Q., Vargas, J. and Lenzi, A., Time-harmonic analysis of acoustic pulsation in gas pipeline systems using the Finite Element Transfer Matrix Method: Theoretical aspects, *Mechanical Systems and Signal Processing*, **186**, 109824, (2023). https://doi.org/10.1016/j.ymssp.2022.109824

[27] Cao, Y. H., Liu, G. M. and Hu, Z., Vibration calculation of pipeline systems with arbitrary branches by the hybrid energy transfer matrix method, *Thin-Walled Structures*, **183**, 110442, (2023). https://doi.org/10.1016/j.tws.2022.110442

[28] Lin, J. Z., Zhao, Y. L., Zhu, Q. Y., Han, S., Ma, H. and Han, Q. K., Nonlinear characteristic of clamp loosing in aero-engine pipeline system, *IEEE ACCESS*, **9**, 64076-64084, (2021). https://doi.org/10.1109/ACCESS.2021.3073561

[29] Chen, W. J., Cao, Y. M., Guo, X. M., Ma, H., Wen, B. C. and Wang, B., Nonlinear vibration analysis of pipeline considering the effects of soft nonlinear clamp, *Applied Mathematics and Mechanics*, **43**(10), 1555-1568, (2022). https://doi.org/10.1007/s10483-022-2903-7

[30] Yang, Y. B., Sui, G. H. and Zhang, Y. H., Response spectrum method for fatigue damage assessment of aero hydraulic pipeline systems, *Computers and Structures*, **287**, 107119, (2023). https://doi.org/10.1016/j.compstruc.2023.107119

[31] Zhang, Y., Sun, W., Ji, W. H. and Wang, B., Hoop layouts optimization for vibration reduction of L-shaped pipeline based on substructure-analytical model and genetic algorithm, *Journal of the Brazilian Society of Mechanical Sciences and Engineering*, **45**, 243, (2023). https://doi.org/10.1007/s40430-023-04131-y

[32] Dou, B., Ding, H., Mao, X. Y., Wei, S. and Chen, L. Q., Dynamic modeling of fluid-conveying pipes restrained by a retaining clip, *Applied Mathematics and Mechanics*, **44**(8), 1225-1240, (2023). https://doi.org/10.1007/s10483-023-3016-9

[33] Ma, H. W., Sun, W., Ji, W. H., Zhang, Y., Liu, X. F. and Liu, H. H., Dynamic modeling and vibration analysis of planar pipeline with partial constrained layer damping treatment: Theoretical and experimental studies, *Composite Structures*, **323**, 117476, (2023). https://doi.org/10.1016/j.compstruct.2023.117476

[34] Ma, H. W., Sun, W., Ji, W. H., Liu, X. F., Liu, H. H. and Du, D. X., Nonlinear vibration analysis of Z-shaped pipes with CLD considering amplitude-dependent characteristics of clamps, *International Journal of Mechanical Sciences*, **262**, 108739, (2023). https://doi.org/10.1016/j.ijmecsci.2023.108739

[35] Xu, Y. L., Zhang, L., Wei, H., Zhang, Z. L., Yang, F., Hu, H. P. and Hu, Y. T., Nonlinear dynamics of viscoelastic fluid-conveying pipe installed within uniform external cross flow by pipe clamps, *Applied Ocean Research*, **135**, 103547, (2023). https://doi.org/10.1016/j.apor.2023.103547

[36] Chen, W. J., Cao, Y. M., Chen, S., Guo, X. M., Ma, H. and Wen, B. C., Semi-analytical dynamic modeling of parallel pipeline considering soft nonlinearity of clamp: A simulation and experimental study, *Mechanical Systems and Signal Processing*, **201**, 110648, (2023). https://doi.org/10.1016/j.ymssp.2023.110648

[37] Zhang, Y., Sun, W., Ma, H. G., Ji, W. H. and Ma, H., Semi-analytical modeling and vibration analysis for U-shaped, Z-shaped and regular spatial pipelines supported by multiple clamps, *European Journal of Mechanics/A Solids*, **97**, 104797, (2023). https://doi.org/10.1016/j.euromechsol.2022.104797

[38] Chai, Q. D., Zeng, J., Ma, H., Li, K. and Han, Q. K., A dynamic modeling approach for nonlinear vibration analysis of the L-type pipeline system with clamps, *Chinese Journal of Aeronautics*, **33**(12), 3253-3265, (2020). https://doi.org/10.1016/j.cja.2020.04.007

[39] Cao, Y. M., Chen, W. J., Ma, H., Li, H., Wang, B., Tan, L., Wang, X. and Han, Q. K., Dynamic modeling and experimental verification of clamp–pipeline system with soft nonlinearity, *Nonlinear Dynamics*, **111**(19), 17725-17748, (2023). https://doi.org/10.1007/s11071-023-08814-y

[40] Cao, Y. M., Chai, Q. D., Guo, X. M., Ma, H. and Wang, P. F., Comparative study on two finite element models for multi-clamp pipeline system, *Journal of Mechanical Science and Technology*, **36**(3), 1157-1169, (2022). https://doi.org/10.1007/s12206-022-0208-5

[41] Cao, Y. M., Guo, X. M., Ma, H., Ge, H., Li, H., Lin, J. Z., Jia, D., Wang, B. and Ma, Y. C., Dynamic modelling and natural characteristics analysis of fluid conveying pipeline with connecting hose, *Mechanical Systems and Signal Processing*, **193**, 110244, (2023). https://doi.org/10.1016/j.ymssp.2023.110244

[42] Ji, W. H., Sun, W., Ma, H. W., Zhang, Y. and Wang, D., A high-precision super element used for the parametric finite element modeling and vibration reduction optimization of the pipeline system, *Journal of Vibration Engineering & Technologies*, **12**(2), 1177-1193, (2023).

[43] Ji, W. H., Sun, W., Zhang, Y., Wang, D. and Wang, B., Parametric model order reduction and vibration analysis of pipeline system based on adaptive dynamic substructure method, *Structures*, **50**, 689-706, (2023). https://doi.org/10.1016/j.istruc.2023.02.062

[44] Ma, H. W., Sun, W., Wang, D., Du, D. X., Liu, X. F. and Lin, J. Z., Finite element modeling of straight pipeline with partially attached viscoelastic damping patch based on variable thickness laminated element, *Composite Structures*, **314**, 116944, (2023). https://doi.org/10.1016/j.compstruct.2023.116944

[45] Guo, X. M., Xiao, C. L., Ge, H., Ma, H., Li, H., Sun, W. and Liu, Z. H., Dynamic modeling and experimental study of a complex fluid-conveying pipeline system with series and parallel structures, *Applied Mathematical Modelling*, **109**, 186-208, (2022). https://doi.org/10.1016/j.apm.2022.04.003

[46] Guo, X. M., Cao, Y. M., Ma, H., Li, H., Wang, B., Han, Q. K. and Wen, B. C., Vibration analysis for a parallel fluid-filled pipelines-casing model considering casing flexibility, *International Journal of Mechanical Sciences*, **231**, 107606, (2022). https://doi.org/10.1016/j.ijmecsci.2022.107606

[47] Guo, X. M., Gu, J. F., Li, H., Sun, K. H., Wang, X., Zhang, B. J., Zhang, R. W., Gao, D. W., Lin, J. Z., Wang, B., Luo, Z., Sun, W. and Ma, H., Dynamic modeling and experimental verification of an L-shaped pipeline in aero-engine subjected to base harmonic and random excitations, *Applied Mathematical Modelling*, **126**, 249-265, (2024). https://doi.org/10.1016/j.apm.2023.10.046

[48] Liu, Y., Wei, J. T., Du, H., He, Z. P. and Yan, F. C., An analysis of the vibration characteristics of an aviation hydraulic pipeline with a clamp, *Aerospace*, **10**, 900, (2023). https://doi.org/10.3390/aerospace10100900

[49] Lin, J. Z., Niu, Z. H., Zhang, X. F., Ma, H., Zhao, Y. L. and Han, Q. K., Clamp nonlinear modeling and hysteresis model parameter identification, *IEEE Access*, **9**, 147757-147767, (2021). https://doi.org/10.1109/ACCESS.2021.3123469